ACS Photonics

Letter

pubs.acs.org/journal/apchd5

Radiatively Broadened Incandescent Sources

Simon Huppert,[†] Angela Vasanelli,[*,†] Thibault Laurent,[†] Yanko Todorov,[†] Giulia Pegolotti,[†] Grégoire Beaudoin,[‡] Isabelle Sagnes,[‡] and Carlo Sirtori[†]

[†]Laboratoire Matériaux et Phénomènes Quantiques, Sorbonne Paris Cité, Université Paris Diderot, UMR7162, 75013 Paris, France

[‡]Laboratoire de Photonique et de Nanostructures, CNRS, 91460 Marcoussis, France

Supporting Information

ABSTRACT: We study the incandescence of a semiconductor system characterized by a radiatively broadened material excitation. We show that the shape of the emission spectrum and the peak emissivity value are determined by the ratio between radiative and nonradiative relaxation rates of the material mode. Our system is a heavily doped quantum well, exhibiting a collective bright electronic excitation in the mid-infrared. The spontaneous emission rate of this collective mode strongly depends on the emission direction and, uncommonly for an intersubband system, can dominate nonradiative scattering processes. Consequently the incandescence spectrum undergoes strong modifications when the detection angle is varied. Incandescence is modeled solving quantum Langevin equations, including a microscopic description of the collective excitations, decaying into electronic and photonic baths. We demonstrate that the emissivity reaches unity value for a well-defined direction and presents an angular radiative pattern that is very different from that of an oscillating dipole.

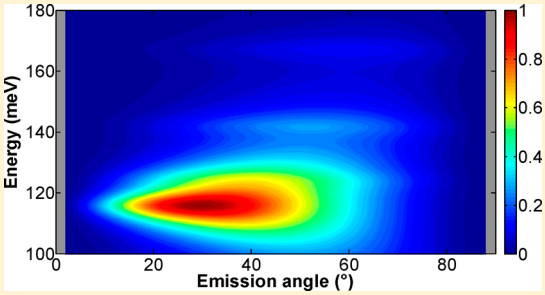

KEYWORDS: *thermal emission, quantum Langevin equations, semiconductor quantum wells, intersubband plasmon, superradiance*

Midinfrared sources are required for many applications such as gas spectroscopy, sensing, imaging, surveillance, and threat detection. Efficient semiconductor light-emitting devices are not available in this spectral region due to extremely long spontaneous emission time as compared to nonradiative scattering processes of electrons in solids. Stimulated emission enables overcoming this issue in quantum cascade lasers,[1] which are based on a system of tunnel coupled semiconductor quantum wells, engineered to achieve population inversion. However, they do not yet fulfill the needs for broadband and cheap sources. Hence, the most common commercial infrared sources are standard incandescent filaments or membranes.

Quasi-monochromatic infrared thermal sources have been developed making use of Kirchhoff's law, which states that the emissivity of a material equals its absorptivity.[2] The latter can be engineered by structuring the surface of an emitter on a subwavelength scale with periodic gratings,[3] photonic crystals,[4,5] and metamaterials.[6] This approach requires an accurate electromagnetic modeling of the photonic structure in order to achieve unity absorptivity at the desired wavelength. Quasi-monochromatic thermal emission has also been obtained by exploiting naturally narrow optical resonances of a material, possibly coupled to photonic structures.[7,8] In particular, electronic transitions between confined states in the conduction band of semiconductor quantum wells (QWs) (intersubband transitions), displaying quasi-monochromatic absorption, can be used to realize controlled incandescent devices.[5,8,9] Quantum wells have also been exploited to demonstrate the first dynamic thermal emission control.[10]

The design of controlled incandescent devices is based on the maximization of the emissivity by means of electromagnetic modeling, including nonradiatively broadened material resonances through a semiclassical description.[7,8,11] However, a microscopic description of the material excitations can give a more in-depth insight on the impact of the different decay mechanisms on the incandescent emission. This has been shown for instance in the temperature-dependent incandescence of rare earth oxide emitters that can only be explained by taking into account radiative and nonradiative relaxation channels in a microscopic model.[12]

In this work we show how the interplay between radiative and nonradiative processes controls the spectral properties of incandescent sources based on highly doped semiconductor quantum wells. Due to the presence of strong carrier−carrier interactions,[13−15] the absorption spectrum of highly doped quantum wells with several occupied subbands presents a single bright mode, the multisubband plasmon (MSP), concentrating most of the oscillator strength of the system.[16,17] These collective excitations display a superradiant behavior, with a density-dependent spontaneous emission rate, that can be evaluated using Fermi's golden rule:[18,19]

$$\frac{1}{\tau_\theta} = \Gamma_0 \frac{\sin^2\theta}{\cos\theta} \text{ with } \Gamma_0 = \frac{e^2 N_s}{2m^* c\varepsilon_0 \sqrt{\varepsilon_s}} \quad (1)$$

Received: July 27, 2015
Published: November 18, 2015

DOI: 10.1021/acsphotonics.5b00415
ACS Photonics 2015, 2, 1663−1668

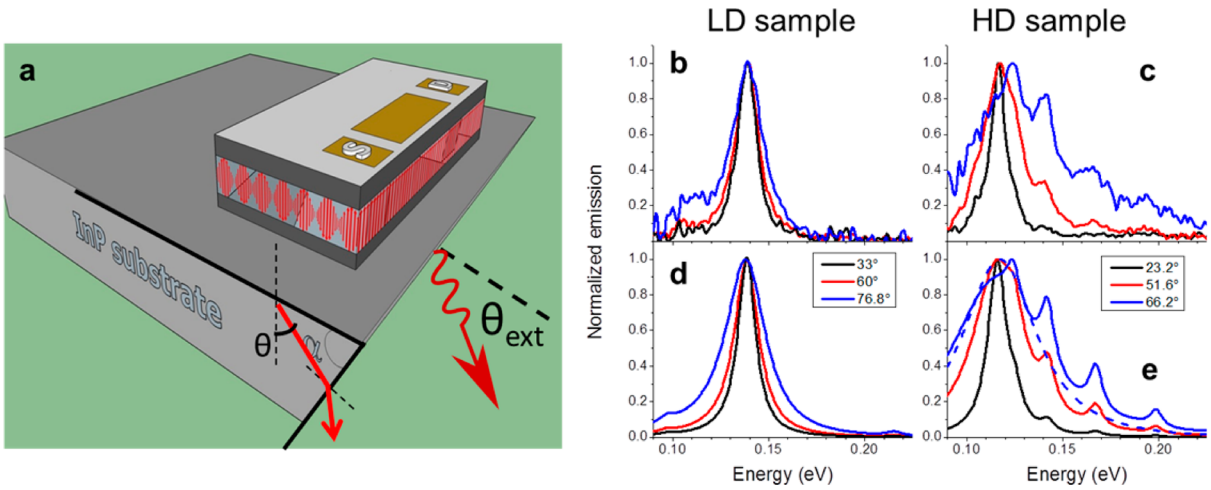

Figure 1. (a) Sketch of the device for angle-resolved emission measurements of electrically injected multisubband plasmons. An in-plane current is injected between the source (S) and the drain (D) of the device, and radiation is extracted from a polished facet (α is the polishing angle). The internal angle for light propagation is indicated with θ, while θ_{ext} represents the external angle. On the side of the mesa we have schematically represented the propagation of the plasmon in the layer plane. Panels (b) and (c) present the normalized measured emission spectra of the two samples at different θ, compared with the simulated ones (shown in panels (d) and (e), solid lines). Dashed line in panel (e) corresponds to single plasmon approximation of the spectrum at 66.2°.

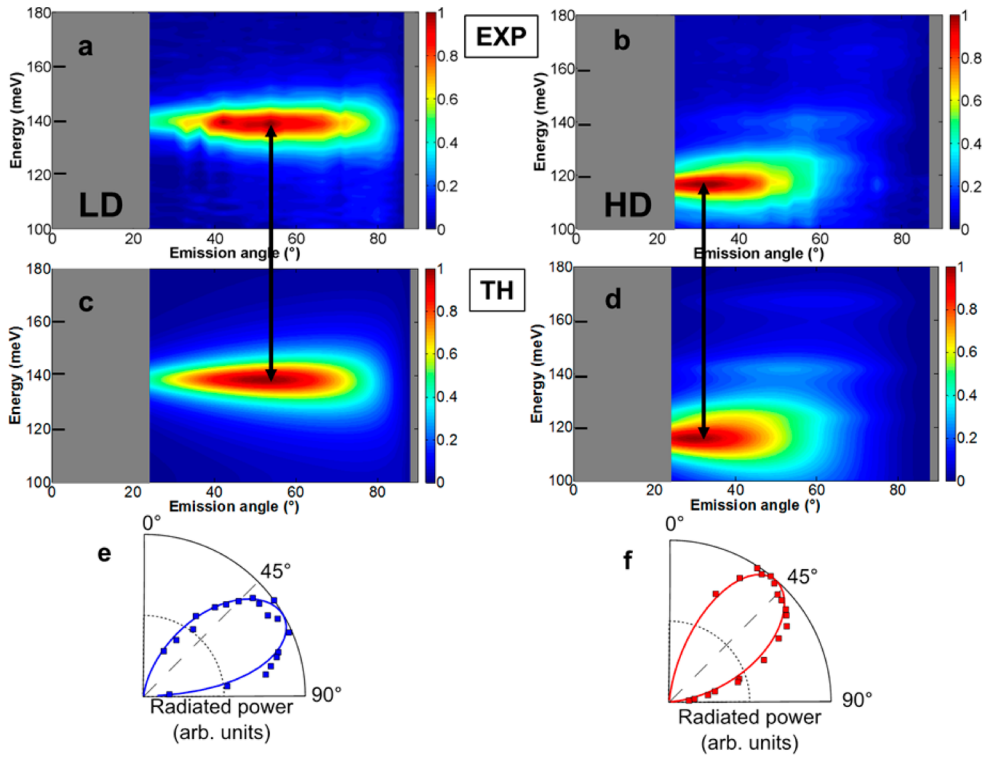

Figure 2. Measured (a and b) and simulated (c and d) color maps of the emitted radiation (in arbitrary units) as a function of the photon energy and of the internal angle θ, for the two samples LD and HD. The black arrows indicate the preferential angle of emission. Panels (e) and (f) present a polar plot of the integrated emitted power as extracted from the measured (squares) and simulated (lines) angle-resolved spectra for samples LD and HD, respectively.

where N_s is the surface electron density, m^* the effective mass, ε_s the semiconductor dielectric constant, and θ the emission angle measured with respect to the normal to the QW plane. In highly doped GaInAs quantum wells the spontaneous emission time can reach few tens of femtoseconds.[18] As this value is much shorter than the characteristic time of any nonradiative scattering event,[20] the energy relaxation dynamics of the plasmon can be dominated by the radiative rate $1/\tau_\theta$. In the following we exploit the strong angular dependence of $1/\tau_\theta$ to prove the importance of collective spontaneous emission for plasmon relaxation. Our complete quantum model of the incandescence, based on the resolution of quantum Langevin equations, is then presented. This model, providing a microscopic description of the incandescence without employing Kirchhoff's law or a dielectric function, perfectly reproduces our experimental results. We finally demonstrate that without

DOI: 10.1021/acsphotonics.5b00415
ACS Photonics 2015, 2, 1663−1668

any photonic structure the emissivity reaches unity value for a well-defined spatial direction as a result of a critical coupling effect, controlled by the matching between spontaneous emission and nonradiative excitation rates.

RESULTS AND DISCUSSION

Our samples are based on a GaInAs/AlInAs highly doped QW grown by metal organic chemical vapor deposition on an InP substrate. The most doped one (named HD) consists of a 100 nm GaInAs layer (embedded between AlInAs barriers) with an electronic density of 7.5×10^{13} cm^{-2}; the second one is composed of an 18.5 nm QW, with an electronic density of 1.2×10^{13} cm^{-2} (named LD). The samples are prepared to perform angle-resolved emission measurements, under application of a current in the QW plane.[21] For this, ohmic NiAuGe/NiAu contacts are diffused down to the QW and the facet of the sample is mechanically polished with an angle α. A Ti/Au layer is deposited on the top surface of the sample, in order to maximize the electromagnetic field overlap with the QW. Figure 1a presents a sketch of the sample geometry with a schematic representation of MSP propagation in the QW plane, characterized by an in-plane wavevector $\vec{k}$. In our experiment, the sample is kept at heat sink temperature $T_0 = 300$ K, while the electron gas is thermally excited by the application of an in-plane current modulated with a square wave at 10 kHz. The current increases the temperature of the electron gas to $T > T_0$. This excites MSPs, which decay by emitting photons with the in-plane wavevector $\vec{k}$ at an angle θ_{ext}. By performing angle-resolved measurements we can therefore access different MSP states.

Figure 1 presents simulated and experimental plasmonic incandescence spectra for different emission angles and doping densities. Figure 1b and c show normalized spectra obtained respectively for samples LD and HD at three different values of the internal emission angle θ. At low θ, the spectra are quasi-monochromatic, with a Lorentzian shape, centered at the energy of the MSP, $\hbar\omega_{MSP}$. The full width at half-maximum is 10 meV for LD (respectively 8 meV for HD), and it is dominated by nonradiative phenomena. When increasing θ, the linewidth gradually increases in a manner that is well described by eq 1. This radiative broadening indicates that photon emission is the most efficient relaxation mechanism for MSPs. Figure 1c also shows resonances at higher energy, appearing for large values of θ; they are due to secondary plasmon modes, which will be discussed further.

It is important to underline that the radiative lifetime calculated from eq 1 varies from 1.4 ps at 20° to 69 fs at 70° for sample LD (respectively from 250 to 12 fs for HD). These dramatic variations not only affect the linewidth, as discussed in ref 18, but also control the emissivity and the radiation directionality in a way that can only be interpreted by accounting consistently for both radiative and nonradiative decay of MSPs. In order to characterize accurately the angular dependence of MSP incandescence, we have measured angle-resolved radiated spectra. Three different polishing angles have been used, in order to cover values of θ ranging from 25° to 85°. Panels (a) and (b) of Figure 2 present the emitted power (in color scale) as a function of the photon energy and emission angle. The emission map has a droplet shape with maximum emission at an angle of ∼55° in the LD sample and ∼35° in the HD sample. A similar conclusion can be drawn by plotting the total emitted power integrated over the detection bandwidth, Figure 2e and f (square symbols): the two samples have distinct preferential emission directions.

This behavior is in apparent contradiction with eq 1, which naturally would provide an evaluation of the emitted power per unit solid angle as

$$dP = \frac{\hbar\omega_{MSP}}{\tau_\theta} n_B(\hbar\omega_{MSP}, T)\, dN_{pl} \tag{2}$$

with $n_B(\hbar\omega_{MSP}, T)$ being the Bose−Einstein distribution for plasmon occupancy at energy $\hbar\omega_{MSP}$ and temperature T, while dN_{pl}, proportional to $\cos\theta\, d\Omega$, is the number of plasmon modes such that their emission direction at resonance is contained in the solid angle of detection $d\Omega$. Equations 1 and 2 would yield a dipole-like emission described by Larmor's formula, i.e., $\sin^2\theta$ dependence with a maximum at $\theta = 90°$, which does not agree with our observations. Indeed eq 2 is obtained assuming that all plasmons thermalize at the temperature T of the heated two-dimensional electron gas. However, plasmons with different wavevector $\vec{k}$ are characterized by different radiative decay rates. This results in a nonequilibrium distribution of plasmons in $\vec{k}$.

We will show in the following that the angular dependence of the emission is a consequence of this nonequilibrium plasmon distribution, due to the interplay between radiative and nonradiative damping. In our model this effect is captured by computing the incandescence spectra through a 2-fold procedure. In a first step the electron−electron interaction is numerically diagonalized to determine the bright MSP modes.[17] These include the main MSP discussed above and secondary modes with much lower oscillator strength. In a second step we solve quantum Langevin equations in an input−output formalism to calculate the emission[22−25] (more details on the model can be found in the Supporting Information). As seen in Figure 1d and e, this method reproduces accurately all the experimental features observed, in particular the angle-dependent broadening, and the appearance of extra peaks beyond $\theta = 40°$ in sample HD. These additional resonances are associated with high-energy plasmon modes issued from the dipole−dipole coupling among intersubband transitions between nonconsecutive levels.[17] It is remarkable that these modes are clearly visible (see also Figure 1c and e), although their oscillator strength is more than 10 times lower than that of the main MSP. The reason for this is that the main emission peak tends to vanish at high θ, while the secondary modes gain in brightness. Figure 2c and d present calculated emission color maps that accurately reproduce the directional emission of both samples (the emission maxima are indicated by arrows in Figure 2).

Analytical results obtained considering only the plasmons with energy $\hbar\omega_{MSP}$ (discarding all secondary MSP modes at higher energy) provide in-depth insights on the physical origin of the directionality of MSP incandescence. In our formalism plasmon emission arises from the coupling of the main MSP with two reservoirs: a hot bath of electronic oscillators, responsible for the creation of plasmons and their nonradiative decay, and a cold bath of photons. The MSP couples to the electronic reservoir at temperature T through a constant damping rate γ, which can be determined from low θ measurements to be 8 and 10 meV for HD and LD, respectively. Conversely the coupling to the photon bath is characterized by a frequency- and angle-dependent rate[22] $\Gamma_\theta(\omega) = \omega/(\hbar\omega_{MSP}\tau_\theta)$. We consider an input of thermal

DOI: 10.1021/acsphotonics.5b00415
ACS Photonics 2015, 2, 1663−1668

excitations in the hot bath at temperature T. The emitted intensity is then calculated from the output photon occupancy, expressed by the following formula:

$$\langle a^{\text{out}\dagger}_{q,\vec{k}} a^{\text{out}}_{q,\vec{k}} \rangle = \alpha_\theta(\omega)\, n_B(\hbar\omega,\, T)$$

$$\alpha_\theta(\omega) = \frac{\frac{4\omega_{MSP}^2}{(\omega_{MSP}+\omega)^2}\gamma\Gamma_\theta(\omega)}{(\omega_{MSP}-\omega)^2 + \frac{4\omega_{MSP}^2}{(\omega_{MSP}+\omega)^2}\left(\frac{\gamma}{2}+\frac{\Gamma_\theta(\omega)}{2}\right)^2} \quad (3)$$

In this relation, ω denotes the frequency of the output photon mode, described by the operator $a^{\text{out}}_{q,\vec{k}}$ (with q the component of the photon wavevector along the growth direction). Antiresonant interaction terms are included in the calculation and are responsible for the factor $4\omega^2_{MSP}/(\omega_{MSP} + \omega)^2$ in eq 3. This term is close to 1 near the resonance, but it becomes significant out of resonance when the radiative broadening is large. Note that $\alpha_\theta(\omega)$ corresponds to the absorbance of the MSP that can be analytically calculated by considering a photonic input in our model. This is exactly what is expected from Kirchhoff's law of thermal emission from nonblack bodies, namely, that the number of emitted photons is the product of the absorbance times the Bose distribution of photons at temperature T with zero chemical potential.[2] Generalization of Kirchhoff's law to nonthermal emission under optical or electrical pumping is discussed in refs 26 and 27.

For fixed values of the dimensionless parameters γ/ω_{MSP} and $kT/(\hbar\omega_{MSP})$, the incandescence spectrum described by eq 3 is a universal function of the coupling ratio $g_\theta = \Gamma_\theta(\omega_{MSP})/\gamma$, which can be decomposed as $g_\theta = g_0\, f(\theta)$, where g_0 is proportional to the electronic density N_s and $f(\theta) = \sin^2\theta/\cos\theta$.

Figure 3 presents the emission spectra calculated for different values of g_θ as a function of the normalized frequency ω/ω_{MSP} (the temperature is such that $kT/(\hbar\omega_{MSP}) = 0.35$). Plasmon incandescence is also compared to the black-body spectrum (black line). Panels (a), (b), and (c) correspond to three different regimes, which can be spanned by changing the detection angle.

For small values of g_θ (Figure 3a), i.e., for low g_0 or θ close to 0°, the spectrum is Lorentzian with a width γ/ω_{MSP} and an amplitude proportional to g_θ. In this case, plasmons are close to equilibrium with the electronic bath, and the power radiated in a solid angle is given by eq 2. Therefore, only the spontaneous emission rate determines the emitted power: the bottleneck phenomenon is in this case the coupling to the photonic bath ("photon bottleneck" regime). The radiated power at a given θ in this regime is proportional to the electronic density in the QW, in agreement with eq 1.

The maximum of $\alpha_\theta(\omega)$ is achieved for $g_\theta = 1$ (Figure 3b), where the MSP emissivity reaches 1 and the emission spectrum coincides at the frequency ω_{MSP} with that of a perfect black body. This situation corresponds to a "critical coupling" regime of incandescence: MSPs are excited at the same rate as they decay radiatively. The plasmon thus plays the role of a spectral filter for the black-body emission, funneling the electronic excitations of the bath toward free space photons.

For $g_\theta > 1$ (Figure 3c), i.e., when spontaneous emission is the dominant relaxation mechanism for the MSP, the linewidth is significantly increased while the peak power decreases. The spectra are deformed from their Lorentzian shape due to several combined effects: the frequency dependence of the Bose−Einstein distribution and of the absorbance and the

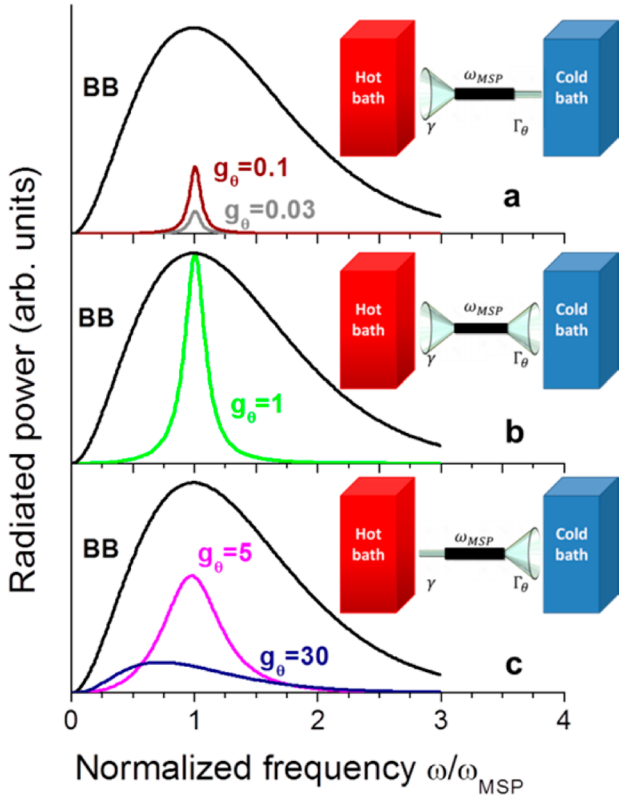

Figure 3. Emission spectra calculated for different values of g_θ as a function of the normalized frequency ω/ω_{MSP} at a temperature such that $kT/(\hbar\omega_{MSP}) = 0.35$ and $\gamma/\omega_{MSP} = 0.05$. Plasmon incandescence is compared to the black-body spectrum (black line). Panels (a), (b), and (c) correspond to the three different regimes described in the main text ((a) photon bottleneck, (b) critical coupling, and (c) electronic bottleneck).

inclusion of the antiresonant interaction terms, which increase $\alpha_\theta(\omega)$ below ω_{MSP} and reduce it above the resonance. The role of the antiresonant terms, similar to that observed in ultrastrongly coupled systems,[22,28] will be examined in more detail in further work. Note that the area under the spectra presented in Figure 3c, obtained for different values of g_θ, does not vary linearly with g_θ, as was the case in the photon bottleneck regime. Indeed, the spontaneous emission time is so short that the MSPs can decay radiatively much faster than they are generated: the bottleneck mechanism is the coupling to the electronic bath ("electronic bottleneck" regime). As a consequence, the MSP occupancy goes to zero for $g_\theta \gg 1$ and thermal equilibrium is reached with the cold bath of photons. The radiated power in solid-angle $d\Omega$ is then approximately expressed as $dP_{g_\theta > 1} = \gamma\hbar\omega_{MSP} n_B(\hbar\omega,T)\, dN_{pl}$, which tends to zero for $\theta \to 90°$ due to the cos θ dependence of dN_{pl}. This explains why the emission is never maximal at 90°, despite the divergence of g_θ.

Figure 4a shows the angular dependence of $g_\theta = g_0\, f(\theta)$ for different values of g_0 corresponding to different electronic densities. Due to the divergence of $f(\theta)$, the critical coupling condition, with unitary emissivity, is always met at a certain angle θ_c, which decreases when g_0 increases. Beyond θ_c, the peak emissivity decreases, as illustrated in Figure 4b for different values of g_0. Finally Figure 4c presents the angular dependence of the integrated radiated power for different values of g_0. For $g_0 \ll 1$ (low electronic density), the system

DOI: 10.1021/acsphotonics.5b00415
ACS Photonics 2015, 2, 1663−1668

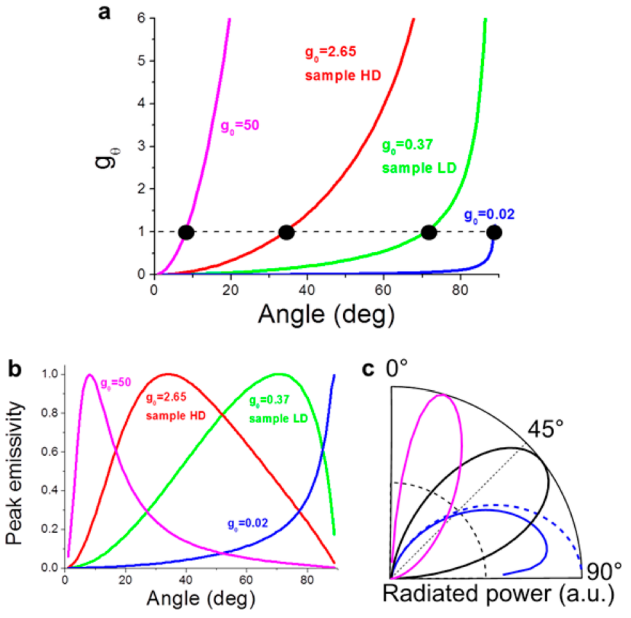

Figure 4. (a) Calculated angular dependence of g_θ for different values of g_0 (i.e., for different electronic densities). The black bullets indicate the values for which the critical coupling condition is met. (b) Angular dependence of the peak emissivity calculated for the same values of g_0 as in panel (a). The value 1 corresponds to critical coupling. (c) Angular dependence of the integrated radiated power for different values of g_0 (solid lines): g_0 = 50 (pink), g_0 = 1 (black), g_0 = 0.02 (blue). The dashed blue line represents the radiated emission of an oscillating dipole, following Larmor's formula.

stays in the photon bottleneck regime until the emission angle is close to 90°. As expected, the radiation angular profile tends to that of a dipole, described by Larmor's formula, i.e., proportional to $\sin^2\theta$ (dashed line). For intermediate densities, the preferential emission direction varies with g_0, getting closer to normal emission for $g_0 \gg 1$, in which case the system stays in the electronic bottleneck regime for almost all values of θ. Therefore, the directionality of the plasmonic incandescence is intrinsically related to the existence of the electronic bottleneck regime induced by the very short spontaneous emission time of the superradiant MSP excitations.

The results presented in this work open entirely new possibilities for designing infrared sources of radiation. The combination of the concepts presented here with the quantum engineering of collective excitations[17] allows spectral and directional control of incandescence. In addition, owing to the very fast temperature response of the electron gas, such sources can be modulated at very high rates. Indeed in our experiment the emission is modulated at 10 kHz through a modulation of the current and therefore of the electronic temperature. Note that we have not observed any variation on the emission signal up to 500 kHz, which corresponds to the cutoff of our mercury cadmium telluride detector. A different approach to dynamically control the thermal emission consists in modulating the emissivity.[10,29] Furthermore, within our theoretical framework the statistical properties of the electronic excitations are naturally related to the quantum fluctuations of the emitted light,[30] which enables quantum-optical investigation of infrared sources. Finally, beyond the context of thermal emission, our model also allows treating the cases of narrowband optical or electronic inputs.[22]

■ ASSOCIATED CONTENT

Supporting Information

The Supporting Information is available free of charge on the ACS Publications website at DOI: 10.1021/acsphotonics.5b00415.

(1) Details on the theoretical model used to compute the incandescence spectra and derivation of eq 3; (2) details on the method used to isolate the plasmonic contribution to the measured incandescence (PDF)

■ AUTHOR INFORMATION

Corresponding Author

*E-mail: angela.vasanelli@univ-paris-diderot.fr.

Notes

The authors declare no competing financial interest.

■ ACKNOWLEDGMENTS

We acknowledge financial support from ERC (grant ADEQUATE), Labex SEAM, Renatech Network, and Agence Nationale de la Recherche (grant ANR-14-CE26-0023-01). We thank Jean-Jacques Greffet for fruitful discussions.

■ REFERENCES

(1) Faist, J.; Capasso, F.; Sivco, D.; Sirtori, C.; Hutchinson, A.; Cho, A. Quantum Cascade Laser. *Science* **1994**, *264*, 553−556.

(2) Greffet, J. J.; Carminati, R.; Joulain, K.; Mulet, J.-P.; Mainguy, S.; Chen, Y. Coherent emission of light by thermal sources. *Nature* **2002**, *416*, 61−64.

(3) Puscasu, I.; Schaich, W. Narrow-band, tunable infrared emission from arrays of microstrip patches. *Appl. Phys. Lett.* **2008**, *92*, 233102.

(4) Pralle, M. U.; Moelders, N.; McNeal, M. P.; Puscasu, I.; Greenwald, A. C.; Daly, J. T.; Johnson, E. A.; George, T.; Choi, D. S.; El-Kady, I.; Biswas, R. Photonic crystal enhanced narrow-band infrared emitters. *Appl. Phys. Lett.* **2002**, *81*, 4685−4687.

(5) De Zoysa, M.; Asano, T.; Mochizuki, K.; Oskooi, A.; Inoue, T.; Noda, S. Conversion of broadband to narrowband thermal emission through energy recycling. *Nat. Photonics* **2012**, *6*, 535−539.

(6) Liu, X.; Tyler, T.; Starr, T.; Starr, A. F.; Jokerst, N. M.; Padilla, W. J. Taming the Blackbody with Infrared Metamaterials as Selective Thermal Emitters. *Phys. Rev. Lett.* **2011**, *107*, 045901.

(7) Jun, Y. C.; Luk, T. S.; Ellis, A. R.; Klem, J. F.; Brener, I. Doping-tunable thermal emission from plasmon polaritons in semiconductor epsilon-near-zero thin films. *Appl. Phys. Lett.* **2014**, *105*, 131109.

(8) Vassant, S.; Archambault, A.; Marquier, F.; Pardo, F.; Gennser, U.; Cavanna, A.; Pelouard, J. L.; Greffet, J. J. Epsilon-Near-Zero Mode for Active Optoelectronic Devices. *Phys. Rev. Lett.* **2012**, *109*, 237401.

(9) Inoue, T.; De Zoysa, M.; Asano, T.; Noda, S. Electrical tuning of emissivity and linewidth of thermal emission spectra. *Phys. Rev. B: Condens. Matter Mater. Phys.* **2015**, *91*, 235316.

(10) Inoue, T.; De Zoysa, M.; Asano, T.; Noda, S. Realization of dynamic thermal emission control. *Nat. Mater.* **2014**, *13*, 928−931.

(11) Inoue, T.; Asano, T.; De Zoysa, M.; Oskooi, A.; Noda, S. Design of single-mode narrow-bandwidth thermal emitters for enhanced infrared light sources. *J. Opt. Soc. Am. B* **2013**, *30*, 165−172.

(12) Torsello, G.; Lomascolo, M.; Licciulli, A.; Diso, D.; Tundo, S.; Mazzer, M. The origin of highly efficient selective emission in rare-earth oxides for thermophotovoltaic applications. *Nat. Mater.* **2004**, *3*, 632−637.

(13) Helm, M.The Basic Physics of Intersubband Transitions. In *Intersubband Transitions in Quantum Wells: Physics and Device Applications I*; Liu, H C.; Capasso, F., Eds.; Academic: San Diego, CA, 2002; Vol. *62*, pp 1−99.

(14) Ando, T.; Fowler, A. B.; Stern, F. Electronic properties of two-dimensional systems. *Rev. Mod. Phys.* **1982**, *54*, 437−672.

DOI: 10.1021/acsphotonics.5b00415
ACS Photonics 2015, 2, 1663−1668

(15) Todorov, Y.; Sirtori, C. Intersubband polaritons in the electrical dipole gauge. *Phys. Rev. B: Condens. Matter Mater. Phys.* **2012**, *85*, 045304.
(16) Delteil, A.; Vasanelli, A.; Todorov, Y.; Feuillet Palma, C.; Renaudat St-Jean, M.; Beaudoin, G.; Sagnes, I.; Sirtori, C. Charge-Induced Coherence between Intersubband Plasmons in a Quantum Structure. *Phys. Rev. Lett.* **2012**, *109*, 246808.
(17) Pegolotti, G.; Vasanelli, A.; Todorov, Y.; Sirtori, C. Quantum model of coupled intersubband plasmons. *Phys. Rev. B: Condens. Matter Mater. Phys.* **2014**, *90*, 035305.
(18) Laurent, T.; Todorov, Y.; Vasanelli, A.; Delteil, A.; Sirtori, C.; Beaudoin, G.; Sagnes, I. Superradiant emission from a collective excitation in a semiconductor. *Phys. Rev. Lett.* **2015**, *115*, 187402.
(19) Alpeggiani, F.; Andreani, L. C. Semiclassical theory of multisubband plasmons: Nonlocal electrodynamics and radiative effects. *Phys. Rev. B: Condens. Matter Mater. Phys.* **2014**, *90*, 115311.
(20) Ferreira, R.; Bastard, G. Evaluation of some scattering times for electrons in unbiased and biased single- and multiple- quantum well structures. *Phys. Rev. B: Condens. Matter Mater. Phys.* **1989**, *40*, 1074−1086.
(21) Maranowski, K. D.; Gossard, A. C.; Unterrainer, K.; Gornik, E. Far-infrared emission from parabolically graded quantum wells. *Appl. Phys. Lett.* **1996**, *60*, 3522−3524.
(22) Ciuti, C.; Carusotto, I. Input-output theory of cavities in the ultrastrong coupling regime: The case of time-independent cavity parameters. *Phys. Rev. A: At., Mol., Opt. Phys.* **2006**, *74*, 033811.
(23) Walls, D. F.; Milburn, G. J. *Quantum Optics*; Springer-Verlag: Berlin,1994.
(24) Gardiner, C. W.; Colett, M. J. Input and output in damped quantum systems: Quantum stochastic differential equations and the master equation. *Phys. Rev. A: At., Mol., Opt. Phys.* **1985**, *31*, 3761−3774.
(25) Cohen-Tannoudji, C.; Dupont-Roc, J.; Grynberg, G. *Atom - Photon Interactions. Basic Processes and Applications*; Wiley: New York, 1998.
(26) Würfel, P. The chemical potential of radiation. *J. Phys. C: Solid State Phys.* **1982**, *15*, 3967−3985.
(27) Manor, A.; Martin, L.; Rotschild, C. Conservation of photon rate in endothermic photoluminescence and its transition to thermal emission. *Optica* **2015**, *2*, 585−588.
(28) Todorov, Y.; Andrews, A. M.; Colombelli, R.; De Liberato, S.; Ciuti, C.; Klang, P.; Strasser, G.; Sirtori, C. Ultrastrong Light-Matter Coupling Regime with Polariton Dots. *Phys. Rev. Lett.* **2010**, *105*, 196402.
(29) Vassant, S.; Moldovan Doyen, I.; Marquier, F.; Pardo, F.; Gennser, U.; Cavanna, A.; Pelouard, J. L.; Greffet, J. J. Electrical modulation of emissivity. *Appl. Phys. Lett.* **2013**, *102*, 081125.
(30) Davidovich, L. Sub-Poissonian processes in quantum optics. *Rev. Mod. Phys.* **1996**, *68*, 127−173.

DOI: 10.1021/acsphotonics.5b00415
ACS Photonics 2015, 2, 1663−1668